Title: Synthesis of $LaWN_3$ nitride perovskite with polar symmetry

Authors: Kevin R. Talley[1,2], Craig L. Perkins[1], David R. Diercks[2], Geoff L. Brennecka[2]*, and Andriy Zakutayev[1]*

Affiliations:

[1] Materials Science Center, National Renewable Energy Laboratory; 15013 Denver West Parkway, Golden, Colorado, 80401, USA

[2] Department of Metallurgical and Materials Engineering, Colorado School of Mines; 1500 Illinois Street, Golden, Colorado, 80401, USA

*Corresponding authors. Emails: Andriy.Zakutayev@nrel.gov, Geoff.Brennecka@mines.edu

Abstract: Oxide materials with the perovskite structure have been used in sensors and actuators for half a century, and halide perovskites transformed photovoltaics research in the past decade. Nitride perovskites have been computationally predicted to be stable, but few have been synthesized, and their properties remain largely unknown. We synthesized and characterized a nitride perovskite lanthanum tungsten nitride ($LaWN_3$) in the form of oxygen-free sputtered thin films, according to spectroscopy, scattering, and microscopy techniques. We report a large piezoelectric response using scanning probe measurements that together with synchrotron diffraction confirm polar symmetry of the perovskite $LaWN_3$. Our $LaWN_3$ synthesis should inspire growth of other predicted nitride perovskites, and measurements of their properties could lead to functional integration with nitride semiconductors for microelectromechanical devices.

One-Sentence Summary: Lanthanum tungsten nitride thin films with perovskite crystal structure and strong piezoelectric response were synthesized

Main Text:

Nitride materials are revolutionizing the way humans access information and communicate with others. For example, 4th generation (4G) wireless networks feature piezoelectric aluminum nitride (AlN) film bulk acoustics resonators (FBARs). Radio-frequency (RF) transistors based on semiconducting gallium nitride (GaN) are becoming an important part of the 5G telecommunication technology. The emerging telecommunication infrastructure would further benefit from improved piezoelectric materials, especially if they are easy to integrate with nitride semiconductors. We synthesized lanthanum tungsten nitride ($LaWN_3$) thin films with a perovskite crystal structure, polar symmetry, and strong piezoelectric response. Synthesis of this nitride member of the broad family of perovskite structured materials with ABX_3 stoichiometry (e.g., oxides, halides, chalcogenides), suggests that other computationally predicted nitride perovskites with useful properties should be also possible to synthesize.

Materials with the perovskite crystal structure (Fig. 1A) are arguably the single most famous class of oxide compounds *(1)*. Oxide perovskites (e.g., $Pb(Zr,Ti)O_3$ (PZT), $(Ba,Sr)TiO_3$ (BST)) with strong piezoelectric response have been extensively used for ceramic capacitors *(2)*, microelectromechanical actuators *(3)*, electrochemical cells *(4)*, and many other applications *(5,6)* over the past century *(7)*. In the past decade, research activity on halide (X = Cl, Br, I) perovskites (e.g. $CH_3NH_3PbI_3$, $CsPbI_3$) has skyrocketed because of their potential application as inexpensive and efficient optoelectronic devices *(8)*. Giant optical anisotropy and nonlinear optics applications have recently attracted attention to chalcogenide (X = S, Se) perovskites (e.g. $BaTiS_3$, $SrTiS_3$) *(9)*. In contrast to oxides, chalcogenides, and halides, very few experimental reports of nitride perovskites exist in crystallographic databases or the literature (Fig. 1B). The few reported perovskites with high nitrogen content include powder $TaThN_3$ synthesized from oxide precursors *(10)*, and powder $LaReN_3$ synthesized from azide precursors *(11)*. Other known inter-metallic materials (e.g. Mg_3SbN, Mn_3CuN) have an anti-perovskite structure and low nitrogen content *(12)*. The relatively low number of reported nitride perovskites is surprising, because pnictide (X = N, P) ABX_3 materials (including perovskites and others) are statistically more likely than the halide ABX_3 materials (Fig. 1B) due to a larger possible number of cation combinations that satisfy -9 collective anion valence versus the combinations for satisfying -3 collective anion valence (Table S1). This leads us to the question of how to discover nitride perovskites and evaluate their potential properties.

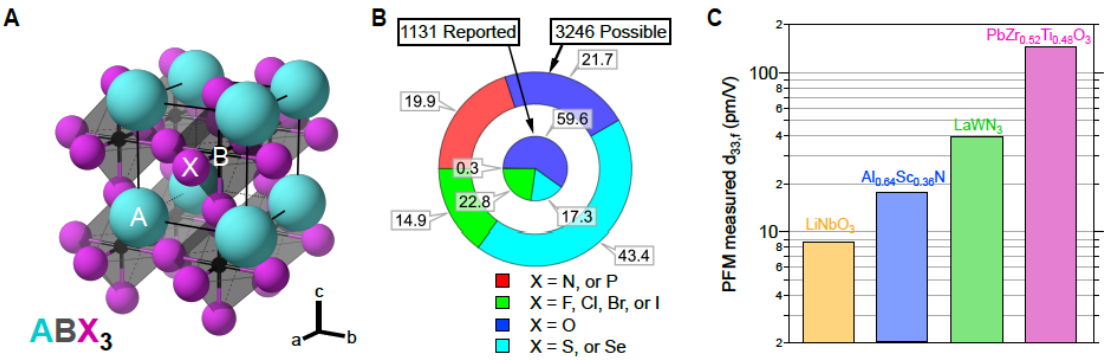

Fig. 1. Nitrides and other materials with the perovskite structure. (A) Cubic ABX_3 perovskite unit cell showing the larger A cation sites and smaller B cation sites in BX_6 octahedra. (B) Comparison of anion diversity in possible charge-balanced vs. experimentally reported

ABX_3 compounds, showing that nitride perovskites are more likely but less reported than halide perovskites. (C) Comparison of materials measured in this report, demonstrating strong piezoelectric response of $LaWN_3$.

Computationally-driven experimental discovery is an effective approach to predict and synthesize new materials *(13)*. In the field of nitrides, we recently synthesized ~10 ternary nitride materials out of ~200 computational predictions *(14)*. Among nitride perovskites, $LnMN_3$ (Ln=La, Ce, Eu, Yb, M=W, Re) materials were predicted by other groups to be thermodynamically stable *(15,16)*, with lanthanum tungsten nitride ($LaWN_3$) having large 350 meV/f.u. formation enthalpy. $LaWN_3$ was also predicted to have ferroelectric properties, with a large 61 $\mu C/cm^2$ spontaneous polarization and a small 110 meV barrier to polarization reversal *(17)*. However, synthesis of $LaWN_3$ by traditional bulk solid state chemistry methods remains extremely challenging *(18)*, often leading to oxynitrides (e.g., $LaWO_{0.6}N_{2.4}$) *(19)*. If pure nitride perovskites can be synthesized, a century of experience in perovskite property engineering *(7)* could be combined with decades of advances in nitride semiconductor integration *(20)*. This would likely have an enormous impact on both fundamental and applied research. We synthesized $LaWN_3$ nitride perovskite with polar symmetry and measured a piezoelectric response comparable to oxide perovskites and much greater than other known nitrides (Fig. 1C).

We used physical vapor deposition (combinatorial co-sputtering) to synthesize crystalline $LaWN_3$ thin films on a heated substrate in ultrahigh vacuum to minimize oxygen contamination, and with a nitrogen plasma source to maximize nitrogen incorporation *(21)*. We detected no measurable oxygen (below 3%) throughout the thickness of films beyond a thin (nm-scale) surface oxide layer (Fig. 2A-D) using Auger electron spectroscopy (AES), even after 72 hours of atmospheric exposure. These measurements were performed for a sample with the cation-stoichiometric composition (La/W=1) as determined by X-ray fluorescence spectroscopy (XRF). However, our AES measurements indicate some nitrogen loss (i.e., 51 at.% instead of 60 at.%) which can be written as $LaWN_{3-x}$ (x=0.5) or $LaWN_{2.5}$. This nitrogen deficiency may result from either preferential N removal during AES depth profiling measurement *(21)*, or the well-known tendency of the perovskite structure to accommodate large anion deficiency *(4,11)*. Our scanning transmission electron microscopy (STEM) measurements with energy dispersive x-ray (EDX) analysis from the cross-section of an identical film (Fig. 2E-H) confirm a polycrystalline microstructure (150-200 nm grain size) and demonstrate chemical homogeneity on the nanometer scale. The corresponding X-ray diffraction (XRD) patterns of the cation-stoichiometric composition (La/W=1) are consistent with the modeled phase-pure perovskite reference pattern, with W or WN and amorphous minor secondary phases at W- and La-rich compositions, respectively (Fig. S1). We performed electrical and optical property measurements as a function of cation composition, which show 10^{-4}-10^4 Ω cm resistivity and 1.0-2.5 eV optical absorption onset with increasing La content (Fig. S2). The upper bound of these measurements is the most representative of $LaWN_3$ due to the optoelectronically inert character of the amorphous lanthanum oxide second phase at La-rich compositions.

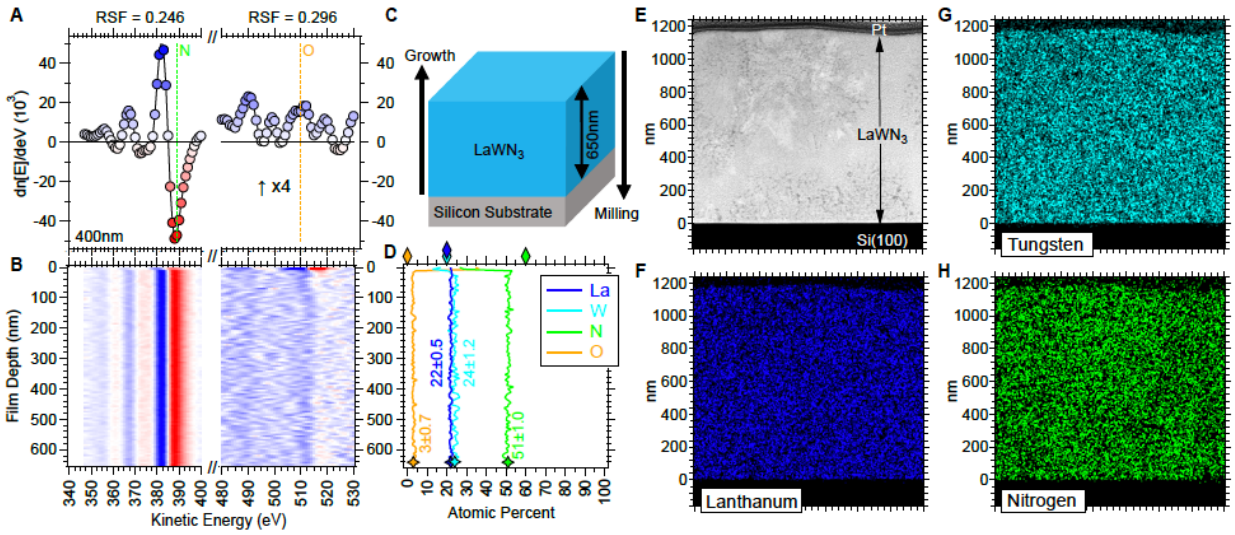

Fig. 2. Chemical composition of $LaWN_3$ thin films. (A) Differentiated AES results and (B) depth-resolved color intensity map for O and N, showing negligible oxygen signal beyond a thin surface layer (RSF = Relative Sensitivity Factor). (C) Depth profile and (D) resulting element concentration for all elements, with the average and ideal composition indicated by stars and diamonds at the bottom and top, respectively. (E-F) STEM and EDX images, showing a polycrystalline microstructure and chemical homogeneity of La, W and N in $LaWN_3$ thin films.

To determine the crystal structure of $LaWN_3$, we synthesized randomly-oriented polycrystalline thin films by rapid thermal annealing (RTA) of atomically-dispersed amorphous La-W-N precursor films. These samples were sputter deposited on glass substrates and protected from oxidation with an AlN capping layer *(21)*. The capped amorphous sample libraries were also free of oxygen (Fig. S3) and had a distinct color change close to the La/W=1 composition (Fig. S4), from black on the W-rich side to translucent yellow on the La-rich side. This yellow color change is indicative of a <2.5 eV band gap. Following the RTA, we observed a randomly-oriented polycrystalline microstructure that was evident from uniform Debye-Scherrer rings (Fig. 3A). Our Rietveld refinement of the integrated XRD patterns (Fig. 3B) shows a majority perovskite phase along with a minority metallic tungsten (W) phase (<5% by volume) and possibly WN phase (<1%) (Table S2). For the perovskite crystal structure refinement, we chose candidate space groups (Table S3) calculated to be within ~100 meV/f.u. of the lowest energy predicted R3c symmetry of $LaWN_3$ *(17)*, as well as the higher energy $I\bar{4}$ space group reported for the $LaWO_{0.6}N_{2.4}$ oxynitride perovskite (*19*). The structure refinement, performed for the unit cell lattice vectors and angles with all other variables held constant, resulted in low and statistically indistinguishable residuals for both the rhombohedral (R3c, space group 161) and tetragonal ($I\bar{4}$, space group 82) symmetries (Fig. S5). We refined lattice parameters of the ground state R3c perovskite structure to be a = 5.64A, $\alpha = 60.33^{o}$ in rhombohedral notation (*21*), and a = 5.67A, c = 13.79 in hexagonal notation, consistent with theoretical prediction for $LaWN_3$ (*17*). Our TEM-based selected area electron diffraction (SAED) results (Fig. 3C-F) confirmed the perovskite structure that we determined by XRD, and were similarly unable to resolve the non-polar $I\bar{4}$ (SG 82) versus polar R3c (SG 161) structural distortions.

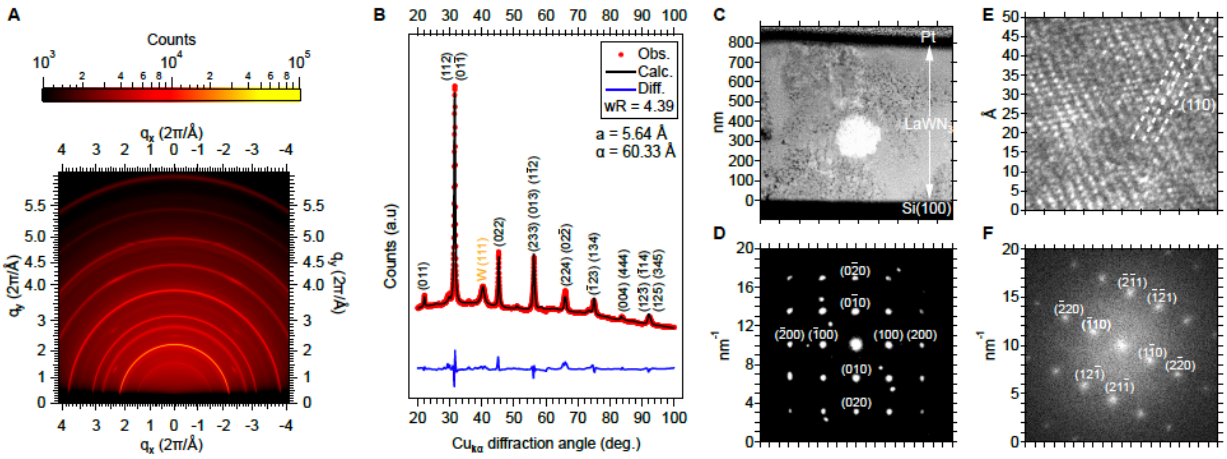

Fig. 3. Crystal structure of $LaWN_3$ thin films. (A) Two-dimensional XRD pattern, indicating randomly oriented polycrystalline microstructure. (B) Rietveld refinements of XRD data for $LaWN_3$ thin films with a predicted rhombohedral unit cell of R3c symmetry (space group 161) and bcc-W minority phase (<5% by volume). (C) STEM-HAADF (high angle annular dark field) image of an as-deposited crystalline film highlighting a single grain (in white), and (D) SAED from this grain showing a pseudo-cubic perovskite [001] type pattern. (E) High resolution image of a single grain showing the pseudo-cubic (011) lattice spacing and (F) the associated fast Fourier transform of (E) indexed with a pseudo-cubic [113] type pattern.

To distinguish between the two possible polar and non-polar symmetries of $LaWN_3$ (*17*,*19*), we conducted piezoresponse force microscopy (PFM) measurements (*21*) of the crystalline $LaWN_3$ film synthesized on the heated substrate (Fig.1, Fig. S1-2). We used a <25 nm tip radius to probe the electromechanical response of uncapped crystalline thin films that were insulating according to conductive atomic force microscopy (c-AFM) measurements (Fig. S6). Our PFM results show qualitatively unambiguous piezoelectric response (Fig. 4A-F), with 65% of >4k pixels in a map (Fig. 4D) having R^2>0.8 fit of piezoelectric amplitude versus drive voltage (Fig. 4E). Our statistical analysis of these measurement results (Fig. 4F) in terms of mean and median of all the pixels with R^2>0.8 indicate $d_{33,f}$ = 40 pm/V magnitude of effective piezoelectric strain coefficient. This $LaWN_3$ value (Fig. 1C) is 4x larger than that of the $Al_{0.92}Sc_{0.8}N$ (~10 pm/V) and $LiNbO_3$ (~10 pm/V) reference samples (Fig. S7-8), yet smaller than the highly engineered $PbZr_{0.52}Ti_{0.48}O_3$ (PZT) reference sample (~150 pm/V) (Fig. S9). Our PFM results clearly indicate a non-centrosymmetric unit cell, supporting the predicted R3c (SG 161) polar symmetry of $LaWN_3$ (*17*), and ruling out $I\bar{4}$ (SG 82) (*19*) as well as other centrosymmetric possibilities within ~100 meV/f.u. from the ground state (Table S3). While we are hesitant to claim quantitative values of piezoelectric coefficient from such PFM measurements (*22*), the results confirm polar symmetry of $LaWN_3$ and indicate its strong piezoelectric response (Fig. 4A-F).

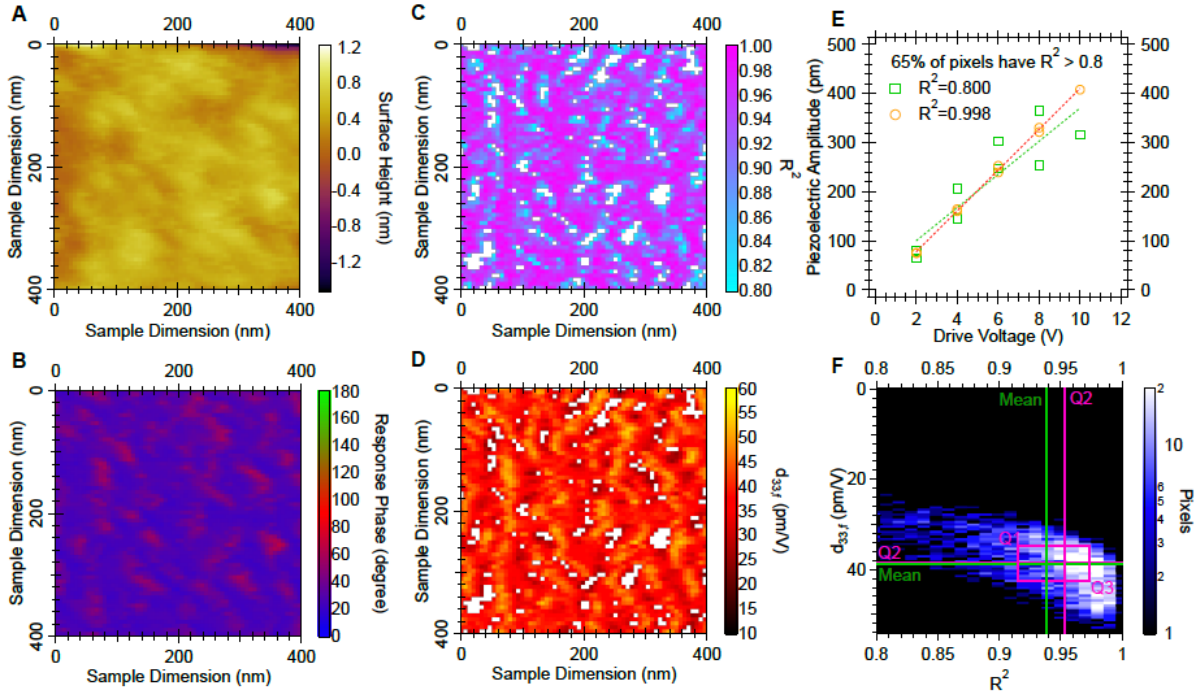

Fig. 4. Piezoelectric properties of $LaWN_3$ thin films. (A) Atomically smooth surface of a single $LaWN_3$ grain, and (B) phase, (C) linearity, (D) slope of each of >4K pixels with $R^2 > 0.8$ for piezoelectric amplitude vs. drive voltage fits. (E) The best and worst fits included in this analysis resulting in (F) a 3D histogram of these $d_{33,f}$ and R^2 values, indicating a mean (green) and median (magenta) value of the piezoelectric response. See supporting information for analysis of $LiNbO_3$, PZT, and $(Al_{0.92}Sc_{0.08})N$ reference samples and details of the PFM measurements (Fig. S7-10).

Considering the computationally predicted ferroelectric character of $LaWN_3$ (17), we attempted to measure $LaWN_3$ polarization reversal (Figs. S10C-D). Our PFM measurements of the crystalline film (*21*) show that the phase of the piezoelectric response of a single 200 nm grain switches in the 0.25 - 0.50 MV/cm range. These values are similar to $PbZr_{0.52}Ti_{0.48}O_3$ (PZT) that we measured under identical conditions (Fig. S10), albeit with 150° instead of 180° phase change indicating either incomplete switching or substantial charged-defect accumulation in the sample. Due to known challenges with such PFM ferroelectric measurements (*22*), we attempted domain writing across 10x10 μm area (Figs. S10E-H), but the results were inconclusive, suggesting the presence of defects at this larger scale. We also attempted macroscale electrical measurements for the samples with a narrow composition gradient and small 100 μm radius contacts (*21*), a process benchmarked by ferroelectric $Al_{1-x}Sc_xN$ thin films synthesized and characterized in our lab (*23*). We deposited these (111)-oriented perovskite films (Fig. S11) on several conductive substrates (i.e., p^+ Si, Pt/Si) under many conditions (e.g., total power, gas ratio, film thickness, etc.) meant to simultaneously maximize crystallinity and minimize conductivity (Fig. S11A). Despite multiple persistent attempts, we observed no definitive polarization-field (P-E) ferroelectric loops up to the measurement field of ~1 MV/cm, with the signal dominated by leakage current (Fig. S11B). These microscale and macroscale electrical measurements are difficult due to a combination of residual minor impurities (e.g., metallic W or WN measured by

XRD) and point defects (i.e., N deficiency suggested by AES). Synthesis of higher-quality $LaWN_3$ (theoretical E_g = 1.8eV) or wider-gap $LaMoN_3$ (theoretical E_g = 2.7 eV) (24) may help decrease the leakage and help determine if these materials are indeed ferroelectric.

Nitride perovskites could substantially extend the range of possible applications of existing commercial nitride semiconductor devices. GaN, AlN and related III-N alloys are well-established for electronics (e.g., radio-frequency transistors), photonics (e.g., light emitting diodes), and telecommunication (e.g., film bulk acoustic resonators) (*20*). Nitride perovskites may offer additional integration advantages compared to oxide perovskites on wurtzite nitrides. High quality epitaxial layers of thermodynamically stable nitride perovskites (similar to oxide perovskites) would be easier to synthesize at high temperature than the recently reported metastable (Al,Sc)N wurtzite alloys with high (>30%) Sc content (*25*,*23*). Also, compared to oxide perovskites, nitride perovskites would be easier to integrate with GaN, similar to other nitride wurtzites. This is because there would be no competing N/O anion exchange reaction resulting in interfacial layer formation known from growth of oxide perovskites on Si (*26*). Thus, epitaxial integration of nitride perovskites on nitride semiconductors may lead to entirely new types of devices for a broad range of applications (*20*), as highlighted by examples of quantum computing and single-photon detectors in superconductor/semiconductor nitride heterostructures (*27*).

Our successful synthesis and characterization of $LaWN_3$ perovskite with polar symmetry should lead to more experimental measurements of its properties, as well as growth and characterization of many other theoretically predicted nitride perovskites. In addition to our measured substantial piezoelectric response (40 pm/V) and theoretically predicted ferroelectricity (*17*), there are multiple theoretical predictions of other interesting and useful $LaWN_3$ properties that await experimental confirmation, including unique spin textures (*28*) and degenerate p-type doping (*24*). The relatively narrow band gap of $LaWN_3$ (theoretical E_g = 1.8 eV) (*24*) compared to oxide perovskites (e.g., 3.4 eV in $BaTiO_3$) could also offer an advantage in studying a controversial topic of solar energy conversion in perovskite materials with polar symmetry (*29*). Other nitride perovskites computationally predicted to have interesting properties are metallic $TbReN_3$ with very high anisotropy and large saturation magnetization (*16*) and $TaThN_3$ with topological insulating behavior (*30*). Nitride perovskites may also harbor other emergent properties or hidden states due to the mixed covalent/ionic character of the metal-nitrogen bonds that results from smaller electronegativity of N compared to O (*18*). Thus, our work on $LaWN_3$ opens the door to synthesis of other predicted nitride perovskites with exceptional electromechanical, magnetic, optoelectronic, thermoelectric, topological, and quantum properties.

References and Notes

1. A. S. Bhalla, R. Guo, R. Roy, The perovskite structure—a review of its role in ceramic science and technology. *Mat. Res. Innovat.* **4**, 3-26 (2016). doi: 10.1007/s100190000062
2. D. Dimos, C. H. Mueller, Perovskite thin films for high-frequency capacitor applications. *Annu. Rev. Mater. Sci.* **28**, 397–419 (1998). doi: 10.1146/annurev.matsci.28.1.397
3. P. Muralt, R. G. Polcawich, S. Trolier-McKinstry, Piezoelectric thin films for sensors, actuators, and energy harvesting. *MRS Bull.* **34**, 658–664 (2009). doi: 10.1557/mrs2009.177

4. M. Papac, V. Stevanović, A. Zakutayev, R. O'Hayre, Triple ionic–electronic conducting oxides for next-generation electrochemical devices. *Nature Materials* 20, 301-313 (2021). doi: 10.1038/s41563-020-00854-8
5. A. V. Boris, Y. Matiks, E. Benckiser, A. Frano, P. Popovich, V. Hinkov, P. Wochner, M. Castro-Colin, E. Detemple, V.K. Malik, C. Bernhard, Dimensionality control of electronic phase transitions in nickel-oxide superlattices. *Science*. **332**, 937–940 (2011). doi: 10.1126/science.1202647
6. X. Li, T. Qiu, J. Zhang, E. Baldini, J. Lu, A.M. Rappe, K.A. Nelson, Terahertz field–induced ferroelectricity in quantum paraelectric $SrTiO_3$. *Science*. **364**, 1079–1082 (2019). doi: 10.1126/science.aaw4913
7. V. M. Goldschmidt, Die gesetze der krystallochemie. *Naturwissenschaften*. **14**, 477–485 (1926). doi: 10.1007/BF01507527
8. M. M. Lee, J. Teuscher, T. Miyasaka, T.N. Murakami, H.J. Snaith, Efficient hybrid solar cells based on meso-superstructured organometal halide perovskites. *Science*. **338**, 643–647 (2012). doi: 10.1126/science.1228604
9. S. Niu, G. Joe, H. Zhao, Y. Zhou, T. Orvis, H. Huyan, J. Salman, K. Mahalingam, B. Urwin, J. Wu, Y. Liu, Giant optical anisotropy in a quasi-one-dimensional crystal. *Nat. Photonics*. **12**, 392–396 (2018). doi: 10.1038/s41566-021-00875-y
10. N. E. Brese, F. J. DiSalvo, Synthesis of the first thorium-containing nitride perovskite, $TaThN_3$, *J. Solid State Chem*. **120**, 378–380 (1995). doi: 10.1006/jssc.1995.1423
11. S. D. Kloß, M. L. Weidemann, J. P. Attfield, Preparation of Bulk-Phase Nitride Perovskite $LaReN_3$ and Topotactic Reduction to $LaNiO_2$-Type $LaReN_2$ *Angew. Chem. Int. Ed*. **60**, 22260-22264 (2021). doi: 10.1002/anie.202108759
12. R. Niewa, Metal-rich ternary perovskite nitrides, *Eur. J. Inorg. Chem*. **2019**, 3647–3660 (2019). doi: 10.18419/opus-10562
13. S. Curtarolo, G.L. Hart, M.B. Nardelli, N. Mingo, S. Sanvito, O. Levy, The high-throughput highway to computational materials design. *Nat. Mater*. **12**, 191–201 (2013). doi: 10.1038/nmat3568
14. W. Sun, C. Bartel, E. Arca, S. Bauers, B. Matthews, B. Orvañanos, B.R. Chen, M.F. Toney, L.T. Schelhas, W. Tumas, J. Tate, A. Zakutayev, S. Lany, A. Holder, G. Ceder, A map of the inorganic ternary metal nitrides. *Nat. Mater*. **18**, 732–739 (2019). doi: 10.1038/s41563-019-0396-2
15. R. Sarmiento-Pérez, T.F. Cerqueira, S. Körbel, S. Botti, M.A. Marques, Prediction of stable nitride perovskites *Chem. Mater*. **27**, 5957–5963 (2015). doi: 10.1021/acs.chemmater.5b02026
16. J. A. Flores-Livas, R. Sarmiento-Pérez, S. Botti, S. Goedecker, M.A. Marques, Rare-earth magnetic nitride perovskites. *J. Phys. Mater*. **2**, 025003 (2019). doi:10.1088/2515-7639/ab083e
17. Y. W. Fang, C.A. Fisher, A. Kuwabara, X.W. Shen, T. Ogawa, H. Moriwake, R. Huang, C.G. Duan, Lattice dynamics and ferroelectric properties of the nitride perovskite $LaWN_3$, *Phys. Rev. B*. **95**, 014111 (2017). doi: 10.1103/PhysRevB.95.014111
18. F. J. DiSalvo, Solid-state chemistry: aa rediscovered chemical frontier, *Science*. **247**, 649–655 (1990). doi: 10.1126/science.247.4943.649
19. P. Bacher, P. Antoine, R. Marchand, P. L'Haridon, Y. Laurent, G. Roult, Time-of-flight neutron diffraction study of the structure of the perovskite-type oxynitride $LaWO_{0.6}N_{2.4}$ *J. Solid State Chem*. **77**, 67–71 (1988). doi: 10.1016/0022-4596(88)90091-6
20. D. Jena, R. Page, J. Casamento, P. Dang, J. Singhal, Z. Zhang, J. Wright, G. Khalsa, Y. Cho, H.G. Xing, The new nitrides: Layered, ferroelectric, magnetic, metallic and superconducting

nitrides to boost the GaN photonics and electronics eco-system, *Jap. J. Appl. Phys.* **58**, SC0801 (2019). doi: 10.7567/1347-4065/ab147b
21. Materials and Methods are available as Supplementary Materials on Science Online
22. R. K. Vasudevan, N. Balke, P. Maksymovych, S. Jesse, S. V. Kalinin, Ferroelectric or non-ferroelectric: Why so many materials exhibit "ferroelectricity" on the nanoscale, *Appl. Phys. Rev.* **4**, 021302 (2017). doi: 10.1063/1.4979015
23. K. Yazawa, D. Drury, A. Zakutayev, G. L. Brennecka, Reduced coercive field in epitaxial thin film of ferroelectric wurtzite $Al_{0.7}Sc_{0.3}N$, *Appl. Phys. Lett.*, **118** 162903 (2021). doi: 10.1063/5.0043613
24. S. Singh, N. T. Madhvendra, Sr-doped $LaMoN_3$ and $LaWN_3$: New degenerate p-type nitrides, *Journ. Appl. Phys.* 124, 065109 (2018). doi: 10.1063/1.5035135
25. S. Fichtner, N. Wolff, F. Lofink, L. Kienle, B. Wagner, AlScN: A III-V semiconductor based ferroelectric, *J. Appl. Phys.* **125**, 114103 (2019). doi: 10.1063/1.5084945
26. R. A. McKee, F. J. Walker, M. F. Chisholm, Crystalline oxides on silicon: the first five monolayers, *Phys. Rev. Lett.* **81**, 3014 (1998). doi:10.1103/PhysRevLett.81.3014
27. R. Yan, G. Khalsa, S. Vishwanath, Y. Han, J. Wright, S. Rouvimov, D.S. Katzer, N. Nepal, B.P. Downey, D.A. Muller, H.G. Xing, GaN/NbN epitaxial semiconductor/superconductor heterostructures, *Nature*. **555**, 183 (2018). doi: 10.1038/nature25768
28. H. J. Zhao, P. Chen, C. Paillard, R. Arras, Y.-W. Fang, X. Li, J. Gosteau, Y. Yang, L. Bellaiche, Large spin splittings due to the orbital degree of freedom and spin textures in a ferroelectric nitride perovskite, *Phys. Rev. B* **102**, 041203 (2020).
29. M. M., Yang, D. J., Kim, M. Alexe, Flexo-photovoltaic effect, *Science*, **360**, 904-907 (2018). doi: 10.1126/science.aan3256
30. M. C. Jung, K.-W. Lee, W. E. Pickett, Perovskite $TaThN_3$: A large-thermopower topological crystalline insulator, *Phys. Rev. B* **97**, 121104 (2018). doi: 10.1103/PhysRevB.97.121104
31. K. R.Talley, S.R. Bauers, C.L. Melamed, M.C. Papac, K.N. Heinselman, I. Khan, D.M. Roberts, V. Jacobson, A. Mis, G.L. Brennecka, J.D. Perkins, A. Zakutayev, COMBIgor: data-analysis package for combinatorial materials science, *ACS Comb. Sci.* **21**, 537–547 (2019). doi: 10.1021/acscombsci.9b00077
32. J. Ilavsky, Nika: software for two-dimensional data reduction, *J. Appl. Crystallogr.* **45**, 324–328 (2012). doi: 10.1107/S0021889812004037
33. B. H. Toby, R. B. Von Dreele, GSAS-II: the genesis of a modern open-source all purpose crystallography software package, *J. Appl. Crystallogr.* **46**, 544–549 (2013). doi: 10.1107/S0021889813003531
34. C. T. Rueden, J. Schindelin, M.C. Hiner, B.E. DeZonia, A.E. Walter, E.T. Arena, K.W Eliceiri, ImageJ2: ImageJ for the next generation of scientific image data, *BMC Bioinformatics*. **18**, 529 (2017).
35. B. J. Rodriguez, C., Callahan, S.V. Kalinin, R., Proksch, Dual-frequency resonance-tracking atomic force microscopy, *Nanotechnology*. **18**, 475504 (2007). doi: 10.1186/s12859-017-1934-z
36. S. Graulis, D. Chateigner, R.T. Downs, A.F.T. Yokochi, M. Quirós, L. Lutterotti, E. Manakova, J. Butkus, P. Moeck, A. Le Bail, Crystallography Open Database–an open-access collection of crystal structures, *J. Appl. Crystallogr.* **42**, 726–729 (2009). doi: 10.1107/S0021889809016690
37. PDF4+, International Centre for Diffraction Data, (2018).
38. R. D. Shannon, Revised effective ionic radii and systematic studies of interatomic distances in halides and chalcogenides, *Acta Crystallogr. Sect. A.* **32**, 751–767 (2002). doi: 10.1107/S0567739476001551

Acknowledgments:

Funding: This work was authored at the National Renewable Energy Laboratory, operated by Alliance for Sustainable Energy, LLC, for the U.S. Department of Energy (DOE) under Contract No. DE-AC36-08GO28308. Funding provided by Office of Science (SC), Office of Basic Energy Sciences (BES), Materials Chemistry Program, as a part of the Early Career Award "Kinetic Synthesis of Metastable Nitrides" (synthesis and characterization); as well as by the U.S. National Science Foundation (NSF) Designing Materials to Revolutionize and Engineer our Future (DMREF) program (DMREF-1534503), and DARPA Tunable Ferroelectric Nitrides (TUFEN) program (DARPA-PA-19-04-03) (piezoelectric measurements). Use of the Stanford Synchrotron Radiation Lightsource, SLAC National Accelerator Laboratory, is supported by the U.S. Department of Energy, Office of Science, Office of Basic Energy Sciences under Contract No. DE-AC02-76SF00515. The views expressed in the article do not necessarily represent the views of the DOE or the U.S. Government.

Author contributions: KRT synthesized the films, performed x-ray fluorescence and scattering measurements, piezoresponse force microscopy, and drafted the original version of the manuscript. CLP performed Auger Electron Spectroscopy measurements and commented on the manuscript. DRD performed transmission electron microscopy measurements and commented on the manuscript. GLB provided intellectual guidance and physical resources, assisted in data analysis, and edited the manuscript. AZ conceived the overall study, assisted in data analysis, provided intellectual guidance and physical resources; edited, revised and finalized the manuscript.

Competing interests: Authors declare that they have no competing interests.

Data and materials availability: All data are available in the main text or the supplementary materials.

Supplementary Materials

Materials and Methods

Supplemental Text

Tables S1 – S3

Figures S1 – S11

References (31-38)

LaWN3_R3C.cif crystallographic information file